Available online at www.sciencedirect.com
SCIENCE DIRECT®
Journal of Computational Physics 210 (2005) 247–273
JOURNAL OF COMPUTATIONAL PHYSICS
www.elsevier.com/locate/jcp

Modeling extreme waves based on equations of potential flow with a free surface

Dmitry Chalikov [a,*], Dmitry Sheinin [b]

[a] *Earth System Science Interdisciplinary Center (ESSIC), 2207 Comp. and Space Sci. Bldg. 224, University of Maryland, College Park, MD 20742-2465, USA*
[b] *National Center for Environmental Prediction, 5200 Auth Rd., Camp Spring, MD 20746, USA*

Received 15 September 2004; received in revised form 30 March 2005; accepted 4 April 2005
Available online 22 June 2005

Abstract

A method for numerical investigation of nonlinear wave dynamics based on direct hydrodynamical modeling of 1-D potential periodic surface waves is created. The model is a part of an interactive wind–wave model. Using a non-stationary conformal mapping, the principal equations are rewritten in a surface-following coordinate system and reduced to two simple evolutionary equations for the elevation and the velocity potential of the surface; Fourier expansion is used to approximate these equations. High accuracy was confirmed by validation of the non-stationary model against known solutions, and by comparison between the results obtained with different resolution in the horizontal. The method developed is applied to the simulation of waves evolution with different initial conditions. Numerical experiments with initially monochromatic waves with different steepness show that the model is able to simulate breaking conditions when the surface becomes a multi-valued function of the horizontal coordinate. An estimate of the critical initial wave height that divides between non-breaking and eventually breaking waves is obtained. Simulations of nonlinear evolution of a wave field is represented initially by two modes with close wave numbers (amplitude modulation) and a wave field with a phase modulation. Both runs result in the appearance of large and very steep waves, these also break if the initial amplitudes are sufficiently large.
© 2005 Elsevier Inc. All rights reserved.

1. Introduction

This paper describes the results of numerical simulation of multi-mode wave field based on a scheme developed by Chalikov and Sheinin [12,13]. This scheme is specifically oriented to coupled simulations

* Corresponding author.
E-mail address: dchalikov@essic.umd.edu (D. Chalikov).

0021-9991/$ - see front matter © 2005 Elsevier Inc. All rights reserved.
doi:10.1016/j.jcp.2005.04.008

of waves and Wave Boundary Layer (WBL) [6]. This coupled model has been completed and numerical investigation of coupled wind–wave dynamics is underway. This problem has been intensively investigated experimentally, theoretically, and numerically (see [23,4]). All numerical investigations, based on Reynolds equations (started by Gent and Taylor [31], and Chalikov [7]) were performed for 2-D turbulent flow above monochromatic waves. They therefore refer to essentially steady motion. Applications of monochromatic experimental and theoretical results for real nonlinear and multi-mode wave fields were based on linear assumption, assuming that all variables may be obtained by simple superposition of modes with different amplitudes. This assumption is problematic. Preliminary data show that decreasing of wave-induced pressure in a downwind wave slope depends nonlinearly on wave steepness. Accordingly, for correct simulation of wind–wave dynamic interaction a surface should have realistic geometry and valid statistical properties.

Because the development of waves (spectrum evolution) occurs at distances which are much larger, than length of dominant wave, the periodic boundary conditions have been used. This assumption simplifies the construction of a numerical scheme by making possible the application of the Fourier transform method. In this study, we consider 1-D nonlinear waves only. The scheme developed in this study is very exact, allowing us to produce the simulation of wave fields for periods much longer than the period of the dominant wave. This is important because development of statistically steady structure of WBL occurs during many periods of the dominant wave.

The main advantage of the potential motion approximation is that the system of Euler equations is reduced to the Laplace equation. However, the solution to the flow problem of surface wave motion is complicated by the requirement of having to apply the kinematics and dynamic boundary conditions (both nonlinear) on the free surface, the location of which is unknown at any given moment.

The problem of numerical simulation of surface waves has a long history. The most general approach to simulate a motion with a free surface is based on a marker and cell (MAC) method [32] which assumes the tracing of variable surface in a fixed grid with different order accuracy (for example, [44,36,47,43]). At present, applicability of this method is restricted by simulation over relatively short-term periods. However, accuracy of this method will increase significantly when very high resolution become possible. An advantage of this method is that it can be used for simulation of 3-D rotational motion of viscous fluid even for non-single value interface. A motion with a single-value 1-D and 2-D interface is readily simulated using simplest surface-following coordinates $(x, y, z - \eta(x, y))$, where (x, y, z) are Cartesian coordinates and η is a surface elevation [7]. This system of coordinates is unsteady and non-orthogonal, so equations of motion become complicated. Still, this method was effectively applied for simulation of interaction of waves with a shear flow by Dimas and Triantafyllou [17]. Evidently, this approach may be joined with the MAC method, applied locally in the intervals with large steepness. Waves on finite depth have been investigated by transforming the volume occupied by fluid into a rectangular domain [21]. Much more complicated surface-following transformations have been constructed, even for the case of a multiple-valued surface [56]. Grid method was generalized with adaptive grids (e.g. [30]) and in finite-volume approach [27].

Fortunately, many observed properties of surface waves are reproduced well on a basis of a potential approach, which makes possible a reduction by 1 a dimensionality. The numerical methods for inviscid free-surface flow have been reviewed by Mei [41], Yeung [63] and Hyman [34], and for viscous flows by Floryan and Rasmussen [35]. The most recent review of numerical methods for incompressible nonlinear free-surface flow was presented by Tsai and Yue [57]. We limit the scope of this review to those works published after the last mentioned review, which is devoted to free periodic waves and based on the principal equation for potential waves.

The simulation of nonlinear unsteady potential flow with a free surface began with the development of the Eulerian–Lagrangian boundary integral equations by Longuet-Higgins and Cokelet [38] for steep overturning waves. The instability of waves was generated by asymmetric pressure applied on a surface. This method, in principle, may be generalized for 3-D motion, but it demands the considerable computational resources. A boundary method based on the Cauchy integral formulation for 2-D problem was developed

by Vinje and Brevig [58], Baker et al. [1] and Roberts [48]. This method was used by Tanaka et al. [53], who studied the instability and breaking of a solitary wave. Dommermuth et al. [20] compared the solution based on the Cauchy integral method with precise measurements in an experimental wave tank. Good agreement was obtained. The boundary integral method was extended by Dold and Peregrine [18] (hereafter DP), who constructed the precise scheme for performing a simulation of wave evolution with good conservation of invariants. Detailed description of method was given by Dold [19]. Stability of scheme was confirmed by simulation of a steep Stokes wave for several wave periods. This scheme was used successfully for simulation of nonlinear group effects [33]; of dynamics of steep forced waves [5], and for investigation the onset of breaking [2,51]. An advantage of this scheme is extreme efficiency: reliable results may be obtained with low resolution and with modest computer resources. For short term periods, is possibly to distribute the points non-uniformly; this allows effectively to reproduce a sharpening and overturning of waves. In order to increase stability, the authors applied very selective smoothing. Dold [19] noted, however, that for long-term integration the advantage given by non-uniformity of the grid is absent. A sharpening of waves results from nonlinear group effects, which generate a convergence of energy in physical space [51]. It is impossible to predict the location of these events. Nonetheless, Henderson et al. [33] demonstrated excellent results from long-term simulations of nonlinear evolution of wave field with an initially uniform grid.

Another group of numerical methods is based on traditional perturbation expansions (often combined with Fourier transform method); in principle, these include arbitrary high orders of interactions [59,22,60]. However, with increasing steepness, the number of needed Fourier modes in this scheme multiplies. Indeed, this method becomes inapplicable when waves approach overturning. Modification of the high-order spectral method was suggested by Fenton and Rienecker [28].

Craig and Sulem [14] improved stability by use the expansion for vertical velocity instead of potential. This method was later generalized for 2-D potential waves [3]. A numerical scheme for 1-D potential waves based on non-orthogonal surface-following coordinate system and Fourier transform was developed by Chalikov and Liberman [8]. The method is based on iterative transfer of the potential from a fixed coordinate system onto free surface and was used for successful simulation of the bound waves dynamics observed by Yeung [63]. This method is also applicable to 2-D potential waves; however, it becomes ineffective for large numbers of modes with highly variant amplitudes (also true for many methods based on expansions). The reason on this restriction is: the small waves overrun the surface of large waves. The amplitudes of wave disturbances with large wave numbers attenuate with depth so quickly, that they become insignificant at the depth of the order of dominant wave height [64]. In this case, restoring the high-order modes on a free surface becomes inaccurate. However, the high-order perturbation method (and all methods based on the surface-following coordinates) represents a huge step forward from quasi-linear theories based on small-amplitude assumption.

A numerical scheme for direct hydrodynamical modeling of 1-D nonlinear gravity and gravity-capillary periodic waves was developed by Chalikov and Sheinin [9,10,12,13,49]. This scheme is based on conformal mapping of a finite-depth water domain. For the stationary problem, this mapping represents the classical complex variable method (e.g. [15,16]), thought originally developed by Stokes [52]. In a stationary problem the method employs the velocity potential Φ and the stream function Ψ as the independent variables. As we knew recently, a non-stationary conformal mapping was introduced also by Whitney [61], and then was considered by Kano and Nishida [37] and Fornberg [29]. Tanveer [54,55] used this approach for investigation of Rayleigh–Taylor instability and the generation of surface singularities. A new way of deriving equations, a description of a numerical scheme (and its validation) as well as the results of long-term simulations were presented at ONR meeting in Arizona (in 1994). Later, it was described in details by Chalikov and Sheinin [12,13] (hereafter ChSh) and in [50]. The ChSh numerical approach is based on a non-stationary conformal mapping for finite depth which allows rewriting of the principal equations of potential flow with a free surface in a surface-following coordinate system. The Laplace equation retains its form and the

boundaries of the flow domain (i.e. the free surface, and, in the case of finite depth, the bottom) are coordinate surfaces in the new coordinate system. Accordingly, the velocity potential in the entire domain receives a standard representation based on its Fourier expansion on the free surface. As a result, the hydrodynamical system (without any simplifications) is represented by two relatively simple evolutionary equations that can be solved numerically in a straightforward way. The advantages of this approach were briefly discussed by Dyachenko et al. [25]; later the method was used by Zakharov et al. [62] to demonstrate the nonlinear properties of steep waves. In principle, the ChSh method is similar to that based also on conformal mapping as developed by Meiron et al. [42]. These authors concluded that this method is applicable only to "moderately distorted geometry". For simulations of the Stokes wave with peak-to-trough amplitude at 80% of the theoretical maximum, they found that "time stepping errors can cause modulation of the steady waves for times longer than $t = 4\pi$" (time is normalized with the length scale and gravity acceleration). Our scheme allows a simulation the propagation of Stokes wave with amplitude 98% of the maximum for hundreds of periods (and much longer) without noticeable distortions (see Fig. 1). Because Meiron et al. [42] used the same accuracy time stepping scheme as the fourth-order Runge–Kutta scheme used in our work, we conclude that errors in their scheme were produced simply by low resolution: for an approximation of Stokes wave profile just $N = 64$ points were used. We used thousands points. (Zakharov et al. [62] used up to one million Fourier modes.) Another reason on instability might be imprecise approximation of the initial shape of a Stokes wave. We have observed, that the stability of Stokes wave significantly depends on the degree of truncation of Fourier series describing the wave. For example for case $a = 0.42$ (half of crest-to-trough height) the Stokes wave initially assigned by five modes (with resolution 2000 modes, 8000 grid points) disintegrates to time $t = 1$. Exact Stokes wave runs stably the thousands of periods.

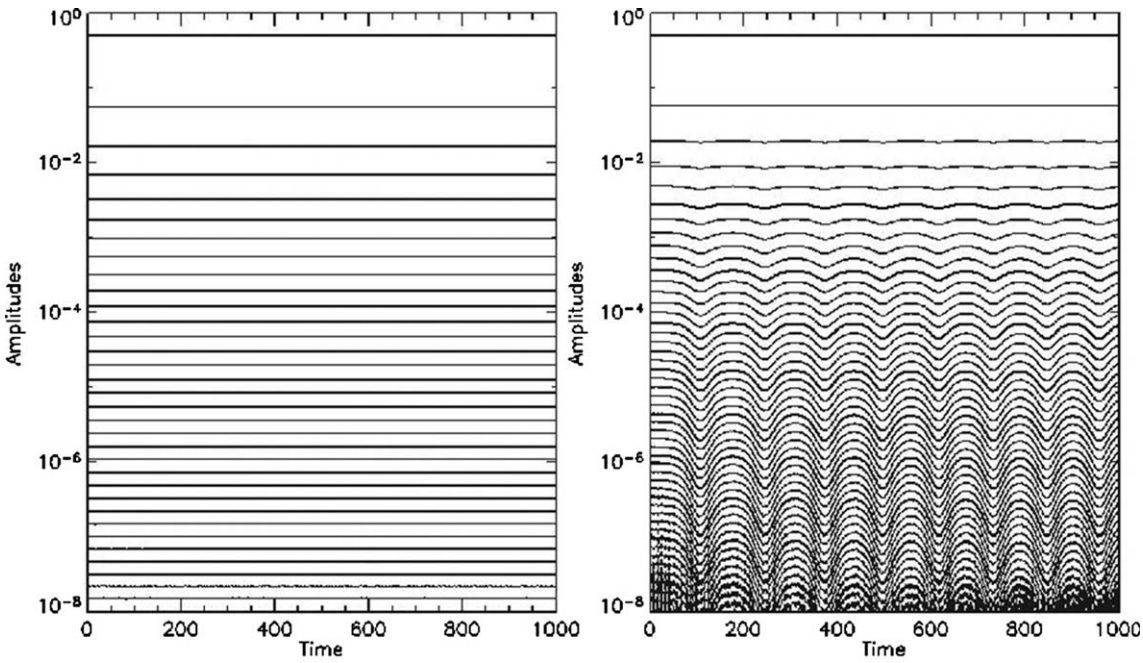

Fig. 1. Long-term evolution of amplitudes of the first 68 Fourier constituents of Stokes waves: $a = 0.42$ (70 constituents, left panel, 1,000,000 time steps) and $a = 0.43$ (96 constituents, right panel) during about 160 periods. The modes with odd numbers are shown in both panels.

Note that a scheme based on high resolution is very fast, so most problems may be investigated with a personal computer.

This model represents a rarity in geophysical fluid dynamics when the equations describing the real process can be solved with a very high accuracy (see Fig. 1). This statement is fully correct if the steepness of waves is not high. Increasing a local steepness often results in a developing of instability thence overturning of sharp crests. Formally, conformal mapping exists up to the moment when overturning volume of water touch the surface (Dyachenko, 2004, personal communication). In such an evolution the number of Fourier modes needed grows very quickly. However, if the special measures (smoothing) are not taken, the calculations usually terminate much earlier, because of strong crest instability (Longuet-Higgins and Dommermuth, [39]), manifested in the splitting of the falling volume into two phases. This phenomenon is obviously non-potential. Hence, as in many branches of geophysical fluid dynamics, special measures must be taken to prevent the numerical instabilities while concurrently accounting on the physical effects of these events.

Our method is applied to the simulation of wave field represented in initial conditions by superposition of running waves with random phases assigned by linear theory. We show that wave fields lose this initial structure and quickly develops new specific features. These features are more pronounced, the larger the nonlinearity of the initial state. Of course, these properties of waves influence significantly the air flow above.

The principal advantage of this scheme is that it combines a concise formulation and computational efficiency with much greater accuracy than the existing schemes. In the case of multi-wave fields *with* wave breaking, the scheme is still applicable if, as it is customary in geophysical fluid dynamics, some dissipation mechanism is included to account for breaking effects while still preventing the numerical instability. Within potential theory, wave breaking can only be parameterized – and it is impossible to simulate all its consequences.

In Section 2, the conformal mapping method is introduced and the principal equations in the new coordinate system are written out. The numerical scheme is described in Section 3. In Section 4, the ability of the model to reproduce a priori known progressive wave solutions is established. Further, validation of model simulations against higher resolution versions is discussed.

The method also is applied to the simulation of extreme waves (Section 5). Two groups of cases are considered: (1) initially monochromatic (harmonic) waves with different steepness; (2) waves with an amplitude modulation (represented initially by two modes with adjacent wave numbers and equal amplitudes), and with a phase modulation. For both types, we observe nonlinear growth and steepening which, if the initial amplitudes are sufficiently large, result in wave breaking. The simulations include the final stages of evolution of the waves as solutions to the potential flow equations when the surface becomes a multi-valued function of the horizontal coordinate.

Finally (Section 6), a possible parameterization of wave breaking is briefly discussed.

2. Equations

Consider the non-dimensional form of the principal 2-D equations for potential waves written in Cartesian coordinates, i.e., the Laplace equation for the velocity potential Φ:

$$\Phi_{xx} + \Phi_{zz} = 0, \tag{1}$$

and the two boundary conditions at the free surface $h = h(x, t)$: the kinematic condition

$$h_t + h_x\Phi_x - \Phi_z = 0, \tag{2}$$

and the Lagrange integral

$$\Phi_t + \frac{1}{2}(\Phi_x^2 + \Phi_z^2) + h + p_e - \sigma h_{xx}(1 + h_x^2)^{-\frac{3}{2}} = 0, \tag{3}$$

where p_e is the density normalized external surface pressure. (Independent variables in subscripts denote partial differentiation with respect to these variables.)

The equations are solved in the domain

$$-\infty < x < \infty, \quad -H \leqslant z \leqslant h(x,t), \tag{4}$$

where H is either a finite depth or infinity. The variables Φ and h are considered to be periodic with respect to x:

$$\Phi(x + 2\pi, z, t) = \Phi(x, z, t), \quad h(x + 2\pi, t) = h(x, t), \tag{5}$$

and normal velocity condition at the bottom is assumed to be zero:

$$\Phi_z(x, z = -H, t) = 0. \tag{6}$$

Eqs. (1)–(3) are written in the non-dimensional form with the following scales: length L, where $2\pi L$ is the (dimensional) period in the horizontal, time $L^{1/2}g^{-1/2}$, and the velocity potential $L^{3/2}g^{1/2}$ (g is the acceleration of gravity). Pressure is taken to be normalized by water density (so its scale is Lg). The last term in Eq. (3) describes the effect of surface tension, and

$$\sigma = \frac{\Gamma}{gL^2}$$

is a non-dimensional parameter ($\Gamma \approx 8 \times 10^{-5}\ \mathrm{m^3\ s^{-2}}$ is the kinematic coefficient of surface tension for water).

System (1)–(6) is solved as an initial value problem for the unknown functions Φ and h with given initial conditions Φ (x, $z = h(x, t = 0)$, $t = 0$) and $h(x, t = 0)$. Note that although Eqs. (2) and (3) are for the free surface, there are no straightforward ways to reduce the problem to a 1-D problem, since, to evaluate Φ_z, one has to solve the Laplace equation (1) in the domain (4) with a curvilinear upper boundary that may be any function of x. This difficulty is known to render integration of the system in Cartesian coordinates either not sufficiently accurate or too expensive, computationally. So, for time periods much greater than the time scale, it is largely impractical. (It is perhaps still more problematic to design an efficient numerical scheme for the stationary version of system (1)–(6).)

To make a numerical solution feasible, we introduce a time-dependent surface-following coordinate system that conformally maps the original domain (4) onto the strip

$$-\infty < \xi < \infty, \quad -\tilde{H} \leqslant \zeta < 0 \tag{7}$$

with a periodicity condition given as

$$\begin{aligned} x(\xi, \zeta, \tau) &= x(\xi + 2\pi, \zeta, \tau) + 2\pi, \\ z(\xi, \zeta, \tau) &= z(\xi + 2\pi, \zeta, \tau), \end{aligned} \tag{8}$$

where τ is the new time coordinate, $\tau = t$.

According to complex variable calculus, conformal mapping (7) → (4) exists and is unique up to an additive constant for x. Note that for the stationary problem, this mapping represents the classic complex variable method (e.g. [16]) originally developed by Stokes [52], employing the velocity potential Φ and the stream function Ψ as the independent variables. In this case, it can be shown that $\Phi = -c\xi + \Phi_0$, $\Psi = c\zeta + \Psi_0$, where $-c$ is the mean velocity at the bottom, with Φ_0 and Ψ_0 as constants. In the non-stationary case, the mapping clearly is time-dependent and no analog of the last relations holds.

It is easily be shown that, due to periodicity condition (8), the required conformal mapping can be represented by Fourier series:

$$x = \xi + x_0(\tau) + \sum_{-M\leqslant k<M, k\neq 0} \eta_{-k}(\tau)\frac{\cosh k(\varsigma+\tilde{H})}{\sinh k\tilde{H}}\vartheta_k(\xi), \tag{9}$$

$$z = \zeta + \eta_0(\tau) + \sum_{-M\leqslant k<M, k\neq 0} \eta_k(\tau)\frac{\sinh k(\varsigma+\tilde{H})}{\sinh k\tilde{H}}\vartheta_k(\xi), \tag{10}$$

where η_k are the coefficients of Fourier expansion of the free surface $\eta(\xi, \tau)$ with respect to the new horizontal coordinate ξ:

$$\eta(\xi,\tau) = h(x(\xi,\zeta=0,\tau), t=\tau) = \sum_{-M\leqslant k\leqslant M} \eta_k(\tau)\vartheta_k(\xi), \tag{11}$$

ϑ_k denotes the functions

$$\vartheta_k(\xi) = \begin{cases} \cos k\xi, & k \geqslant 0, \\ \sin k\xi, & k < 0; \end{cases} \tag{12}$$

M is the truncation number (so far $M = \infty$ is assumed). Non-traditional presentation of Fourier transform with definition (12) is, in fact, convenient for calculations, because $(\vartheta_k)_\xi = k\vartheta_{-k}$ and $\sum(A_k\vartheta_k)_\xi = -\sum kA_{-k}\vartheta_k$. Note that in presentation (12) the indexes $k \geqslant 0$ refer to the real part of the complex presentation and $k < 0$ – the imaginary part. The Fourier coefficients A_k form the array $A(-M:M)$, what makes possible a compact programming in Fortran90.

Time-dependent $x_0(\tau)$ can be chosen arbitrarily, though it is convenient to assume

$$x_0(\tau) = 0. \tag{13}$$

The lower boundary $\zeta = -\tilde{H}$ cannot be chosen arbitrarily, since the relation

$$z(\xi, \zeta = -\tilde{H}, \tau) = -H \tag{14}$$

must hold which, after substituting expansion (10), yields

$$\tilde{H} = H + \eta_0(\tau). \tag{15}$$

Since η_0 is determined by the Fourier expansion (11) and, generally, is an unknown function of time, $\tilde{H}$ also is time-dependent.

Due to conformity of the mapping, Laplace equation (1) retains its form in (ξ, ζ) coordinates. Simple derivations based on the systematic use of Cauchy–Riemann conditions show that system (1)–(3) can be written in the new coordinates, as follows:

$$\Phi_{\xi\xi} + \Phi_{\zeta\zeta} = 0, \tag{16}$$

$$-z_\xi x_\tau + x_\xi z_\tau = \Phi_\zeta, \tag{17}$$

$$\Phi_\tau - J^{-1}(x_\xi x_\tau + z_\xi z_\tau)\Phi_\xi + \frac{1}{2}J^{-1}(\Phi_\xi^2 - \Phi_\zeta^2) + z + p_e - \sigma J^{-3/2}(-x_{\xi\xi}z_\xi + z_{\xi\xi}x_\xi) = 0, \tag{18}$$

where (17) and (18) are written for the surface $\zeta = 0$ (so that $z = \eta$ as represented by expansion (11)), and

$$J = x_\xi^2 + z_\xi^2 = x_\zeta^2 + z_\zeta^2 \tag{19}$$

is the Jacobian of the transformation. Boundary condition (6) is rewritten as

$$\Phi_\zeta(\xi, \zeta = -\tilde{H}, \tau) = 0. \tag{20}$$

The solution to the Laplace equation (16) with boundary condition (20) is readily yielded by Fourier expansion, which reduces system (16)–(18) to a 1-D problem:

$$\Phi = \sum_{-M\leqslant k\leqslant M} \phi_k(\tau)\frac{\cosh k(\zeta+\tilde{H})}{\cosh k\tilde{H}}\vartheta_k(\xi), \tag{21}$$

where ϕ_k are Fourier coefficients of the surface potential Φ (ξ, $\zeta = 0$, τ). Thus, Eqs. (17) and (18) constitute a closed system of prognostic equations for the surface functions $z(\xi, \zeta = 0, \tau) = \eta(\xi, \tau)$ and $\Phi(\xi, \zeta = 0, \tau)$. (It may also be regarded as a system of ordinary differential equations for the Fourier coefficients η_k, ϕ_k. Its explicit form would be somehow complicated; however, it is not needed, since, as described in the next section, we use the Fourier transform method to calculate the nonlinearities.)

System (17), (18) is not resolved with respect to the time derivative of the surface elevation $\eta(\xi, \tau)$. During numerical integration of the initial value problem, the values of the time derivative can be obtained with a simple iterative algorithm, making use of Eq. (17) and Cauchy–Riemann relations $x_{\tau\xi} = z_{\tau\zeta}$, $x_{\tau\zeta} = -z_{\tau\xi}$. However, a more efficient approach may be applied (see ChSh for references). This approach is based, in fact, on mutual dependence the fluctuating components in definitions the conformal coordinates(ξ, ζ). Introducing complex variables $\rho = \xi + \mathrm{i}\zeta$, $r(\rho, \tau) = x(\xi, \zeta, \tau) + \mathrm{i}z(\xi, \zeta, \tau)$ and denoting

$$F(\xi,\zeta,\tau) = \mathrm{Re}\left(\frac{r_\tau}{r_\rho}\right), \quad G(\xi,\zeta,\tau) = \mathrm{Im}\left(\frac{r_\tau}{r_\rho}\right), \tag{22}$$

Eq. (17) can be rewritten as

$$G(\xi,\zeta=0,\tau) = (J^{-1}\Phi_\zeta)_{\zeta=0}. \tag{23}$$

Note that, due to conformity of the transformation, $r(\rho, \tau)$ is an analytic function of ρ. So are $r_\tau = x_\tau + \mathrm{i}z_\tau$, $r_\rho = x_\xi + \mathrm{i}z_\xi$ and their ratio in (22). Therefore, the functions F and G are bound by the Cauchy–Riemann relations:

$$F_\xi = G_\zeta, F_\zeta = -G_\xi. \tag{24}$$

Considering that G is a harmonic function of ξ and ζ and that it goes to zero at the lower boundary $\zeta = -\tilde{H}$ (since JG is equal to the left-hand side of (17), and at that boundary $z = -H$, $z_\tau = z_\xi = 0$), so that

$$(F+\mathrm{i}G)_{\zeta=-\tilde{H}} = \left(\frac{x_\tau}{x_\xi}\right)_{\zeta=-\tilde{H}} = F_{\zeta=-\tilde{H}}, \tag{25}$$

one may write the following expansion:

$$G(\xi,\zeta,\tau) = \sum_{-M\leqslant k\leqslant M, k\neq 0} g_k(\tau)\frac{\sinh k(\zeta+\tilde{H})}{\sinh k\tilde{H}}\vartheta_k(\xi), \tag{26}$$

and relations (24) yield

$$F(\xi,\zeta,\tau) = f_0(\tau) + \sum_{-M\leqslant \kappa\leqslant M, \kappa\neq 0} g_{-k}(\tau)\frac{\cosh k(\zeta+\tilde{H})}{\sinh k\tilde{H}}\vartheta_k(\xi). \tag{27}$$

The function $f_0(\tau)$ can be found using assumption (13), which together with (22) yields (for any ζ and τ):

$$0 = \int_0^{2\pi} x_\tau \,\mathrm{d}\xi = \int_0^{2\pi} (Fx_\xi - Gz_\xi)\,\mathrm{d}\xi;$$

substituting expansions (26), (27), (9), (10), and integrating the products of the Fourier series, we obtain

$$f_0 = \frac{1}{2}\sum_{-M\leqslant k\leqslant M, k\neq 0} k\eta_{-k}\sinh^{-2}k\tilde{H}. \tag{28}$$

Then, if

$$g(\xi,\tau) = G(\xi,\zeta=0,\tau) = \sum_{-M\leqslant\kappa\leqslant M,\kappa\neq 0} g_k(\tau)\vartheta_k(\xi) \tag{29}$$

is known,

$$f(\xi,\tau) = F(\xi,\zeta=0,\tau) = f_0(\tau) + \sum_{-M\leqslant\kappa\leqslant M,\kappa\neq 0} g_{-k}(\tau)\coth(k\tilde{H})\vartheta_k(\xi) \tag{30}$$

is also known: f is a generalization of the Hilbert transform of g which, for $k \neq 0$, may be defined in Fourier space as

$$f_k = g_{-k}\coth k\tilde{H}, \tag{31}$$

whereas f_0 is defined by (28). Thus, we can replace Eq. (17) by explicit expressions for the time derivatives x_τ and z_τ that follow from (22). Finally, Eqs. (17) and (18) can be rewritten as a system resolved with respect to the time derivatives (here $\zeta = 0$):

$$z_\tau = x_\xi g + z_\xi f, \tag{32}$$

$$\Phi_\tau = f\Phi_\xi - \frac{1}{2}J^{-1}(\Phi_\xi^2 - \Phi_\zeta^2) - z - p_e + \sigma J^{-3/2}(-x_{\xi\xi}z_\xi + z_{\xi\xi}x_\xi), \tag{33}$$

where, according to (23),

$$g = (J^{-1}\Phi_\zeta)_{\zeta=0}; \tag{34}$$

f is obtained from g according to (31) and (28); and the derivatives can be expressed through standard differentiation formulae for Fourier series and hyperbolic functions (see ChSh).

Thus, the original system of equations is transformed into two simple evolutionary Eqs. (32) and (33) and diagnostic relations (31) and (34). All equations refer to the free surface and, thus, are essentially 1-D (both spatial derivatives of Φ are obtained by differentiating the series (21)) and can be solved using the Fourier transform method (see Section 3). These equations allow a precise investigation of 1-D periodic potential waves in a broad ranges of two non-dimensional parameters: depth H and capillarity σ.

For deep water ($H = \infty$), the coefficients in expansions (28), (30) and (31) become simpler. The domain (7) turns into the semi-plane $\zeta < 0$ ($z \to -\infty$ when $\varsigma \to -\infty$, a condition which replaces (14)). The conformal mapping (9), (10) acquires the form

$$x = \xi + x_0(\tau) + \sum_{-M\leqslant k<M,k\neq 0} \eta_{-k}(\tau)\exp(k\zeta)\vartheta_k(\xi), \tag{35}$$

$$z = \zeta + \eta_0(\tau) + \sum_{-M\leqslant k<M,k\neq 0} \eta_k(\tau)\exp(k\zeta)\vartheta_k(\xi); \tag{36}$$

the solution (21) of the Laplace equation (16) becomes

$$\Phi = \sum_{-M\leqslant k\leqslant M} \phi_k(\tau)\exp(k\zeta)\vartheta_k(\xi); \tag{37}$$

operator (30) becomes a conventional Hilbert transform and its Fourier space representation (31) and (28) turns into

$$f_k = g_{-k}\operatorname{sign} k \quad (k \neq 0); \qquad f_0 = 0. \tag{38}$$

To process the results of model simulations (Section 5), a diagnostic equation for pressure inside the domain is needed. The standard form for incompressible potential flow is

$$\left(\frac{\partial^2}{\partial x^2} + \frac{\partial^2}{\partial y^2}\right)\left(p + \frac{1}{2}\left(\Phi_x^2 + \Phi_y^2\right)\right) = 0.$$

In the new coordinates, it takes the form:

$$\left(\frac{\partial^2}{\partial\xi^2}+\frac{\partial^2}{\partial\zeta^2}\right)\left(p+\frac{1}{2}J^{-1}\left(\Phi_\xi^2+\Phi_\zeta^2\right)\right)=0. \tag{39}$$

In the absence of capillarity, the upper boundary condition is $p = p_e$. In all model simulations presented herein the prescribed external surface pressure is constant. One may therefore assume

$$p(\xi,\zeta=0,\tau)=p_e=0. \tag{40}$$

In principle, the distribution of surface pressure may be assigned as a function of ξ and τ (what was used, for example by Longuet-Higgins and Cokelet [38]). It is shown below that wave breaking occurs in an adiabatic case when initial conditions correspond to large enough energy. In a coupled wind–wave modeling [6], the surface pressure p_e is a product of solving the equations for air domain.

The lower boundary condition readily follows from the Lagrange integral written for the bottom in the (non-dimensional) Cartesian coordinates: $p_z = -1$. So in the new coordinates, one finds

$$z_\zeta p_\zeta=-J \quad \text{at } \zeta=-\tilde{H}. \tag{41}$$

For deep water, this condition becomes

$$p_\zeta\to-1 \quad \text{at } \zeta\to-\infty. \tag{42}$$

Note that, if for a given moment of time, the velocity potential is constant (the velocity field is identical to zero), the solution to Eq. (39) with boundary conditions (40) and (41) (or, for deep water, (42)) is $p = -\zeta$. Thus, the new vertical coordinate ζ has a certain hydrodynamical sense: $-\zeta$ may be identified with generalized hydrostatic pressure which, by definition, is the pressure in the absence of motion (i.e. the absence of dynamic pressure though not necessarily the state of hydrostatic equilibrium). It is convenient to present the pressure field in terms of its deviation $p + \zeta$ from its generalized hydrostatic component; indeed, this approach is adopted in Section 5.

3. Numerical solution of the principal equations

For spatial approximation of system (32) and (33) we use a Galerkin-type (or "spectral") method based on a Fourier expansion of the prognostic variables with a finite truncation number M. The problem is thus reduced to a system of ordinary differential equations for $4M + 2$ Fourier coefficients $\eta_k(\tau)$, $\phi_k(\tau)$, $-M \leqslant k \leqslant M$:

$$\dot{\eta}_k=E_k(\eta_{-M},\eta_{-M+1},\ldots,\eta_M,\phi_{-M},\phi_{-M+1},\ldots,\phi_M), \tag{43}$$

$$\dot{\phi}_k=F_k(\eta_{-M},\eta_{-M+1},\ldots,\eta_M,\phi_{-M},\phi_{-M+1},\ldots,\phi_M), \tag{44}$$

where E_k, F_k are, respectively, the Fourier expansion coefficients for the right-hand sides of Eqs. (32) and (33) as functions of ξ.

To calculate E_k, F_k as functions of the prognostic variablesη_k, ϕ_k, differentiation of the Fourier series is used (the spatial derivatives are thus evaluated exactly) and the nonlinearities are calculated with the so-called transform method [46,26]), by their evaluation on a spatial grid. If $Y(u(\xi), v(\xi), w(\xi), \ldots)$ is a nonlinear function of its arguments, which are represented by their Fourier expansions, gridpoint values $u(\xi_j)$, $v(\xi_j)$, $w(\xi_j)$, … are first calculated, that is inverse Fourier transforms are performed; after which $Y^{(j)} = Y(u(\xi^{(j)}), v(\xi^{(j)}), w(\xi^{(j)}), \ldots)$ are evaluated at each grid point. Finally, the Fourier coefficients Y_k of the function Y are found by a direct Fourier transform. Here $\xi^{(j)} = 2\pi(j-1)/N$, N is the number of

gridpoints. This approach is exploited extensively in geophysical hydrodynamics, in global atmospheric modeling particularly.

For the method to be a purely Galerkin one, that is to ensure the minimum mean square approximation error, the Fourier coefficients E_k, F_k must be evaluated *exactly* for $-M \leqslant k \leqslant M$. For this purpose, one must choose

$$N > (v+1)M, \tag{45}$$

where v is the maximum order of nonlinearities. Since the right-hand sides of Eqs. (32) and (33) include division by the Jacobian, the nonlinearity is of infinite order such that the above condition on N cannot be met. However, numerical integrations show that if one chooses a value of N ensuring exact evaluation of cubic nonlinearities ($v = 3$ in (45)), a further increase in N (with a fixed M) does not affect the numerical solution. For the results presented in Section 5, $N = 4.5M$ was taken.

However high the spectral resolution might be, long-term simulations of strongly nonlinear waves one must parameterize the energy flux into the severed part of the spectrum ($|k| > M$). If ignored, spurious energy accumulations at large wave numbers may corrupt the numerical solution. Simple dissipation terms were added to the right-hand sides of Eqs. (43) and (44) for this purpose:

$$\dot{\eta}_k = E_k - \mu_k \eta_k, \tag{46}$$

$$\dot{\phi}_k = F_k - \mu_k \phi_k \tag{47}$$

with

$$\mu_k = \begin{cases} rM\left(\frac{|k|-k_d}{M-k_d}\right)^2 & \text{if } |k| > k_d, \\ 0 & \text{otherwise,} \end{cases} \tag{48}$$

where $k_d = M/2$ and $r = 0.25$ were chosen for all the runs discussed below. We found the sensitivity of the results to reasonable variations of k_d and r to be low. The dissipation effectively absorbs energy at wave numbers close to the truncation number M, while leaving longer waves virtually intact, and modes with wave numbers $|k| \leqslant k_d$ unaffected. Note that an increase of the truncation number M shifts the dissipation area to higher wave numbers (and, with $M \to \infty$, the energy sink due to dissipation tends to zero). Therefore, the scheme with the dissipation described retains an approximation of the original (non-dissipative) system.

For time integration, the fourth-order Runge–Kutta scheme was used. The choice of the time step requires special consideration. For any explicit time integration scheme, the stability criterion has the form: $\Delta\tau \leqslant C\omega_{\max}^{-1}$ (if dissipation does not play a major role), where $\Delta\tau$ is the time step, $\omega_{\max}$ is the maximum frequency of the system and C is a constant depending on the scheme. For the Runge–Kutta scheme, $C = 2\sqrt{2}$. For a broad variety of nonlinear problems of hydrodynamics, $\omega_{\max}$ may be estimated from the linear theory: $\omega_{\max} = (\omega_k^{\langle l \rangle})_{\max}$; the linear frequency can be found from the linear dispersion relation, which in our case is

$$\omega_k^{\langle l \rangle} = c_k^{\langle l \rangle} k = \sqrt{(k + \sigma k^3)\tanh kH}, \tag{49}$$

where $(\omega^{\langle l \rangle})_{\max} = \omega_M^{\langle l \rangle}$. However, this approach is impractical (perhaps rendering the scheme unstable) in our case because of strong nonlinear effects – short bound waves[1] propagating with the phase speed of longer free waves. (These effects are extensively considered in ChSh, Section 6.) Instead, an estimate of $\omega_{\max}$

[1] It is well known that in a real wave field the dominate waves have more or less sharp crests and gentle troughs. Naturally, when a routine Fourier presentation is used, to approximate such waves, additional modes are needed. These modes are sometimes called 'bound waves'. This unfortunate expression obscures the essence of the phenomena: real waves evidently are single nonlinear modes, which retain their individuality over time.

suitable for the stability criterion is $\omega_{\max} \approx (c_k^{\langle l \rangle})_{\max} M$ (for deep-water gravity waves this yields $\omega_{\max} \approx c_1^{\langle l \rangle} M = M$, whereas $\omega_{\max}^{\langle l \rangle} = \sqrt{M}$). We note that this estimate is sometimes excessively stringent as a basis for choice of $\Delta\tau$; indeed, the correct relation is $\omega_{\max} = c_{\max}^{[fw]} M$, where $c^{[fw]}$ are (linear) phase speeds of free (carrier) waves capable of having associated bound waves. Such waves may not exist for all the wave numbers. For example, the simulated wave field has only a small portion of energy at wave numbers less than k_0. If $c_k^{\langle l \rangle}$ is a decreasing function of k (as with pure gravity waves), one may use the estimate $\omega_{\max} \approx c_{k_0}^{\langle l \rangle} M$, since wave numbers smaller than k_0 do not carry bound waves, whereas wave numbers greater than k_0 have lower phase speeds. For deep-water gravity waves, this yields $\omega_{\max} \approx M/\sqrt{k_0}$; this estimate is used for the choice of $\Delta\tau$ in the model runs with a narrow initial energy spectrum (Section 5, cases of amplitude and phase modulation).

A separate problem is initial data – normally given in the Cartesian coordinates. These must be converted to the (ξ, ζ) coordinates. For this purpose, an iterative algorithm based on spline fifth-order functions has been developed which carries out the transformation with computer accuracy.

All cases considered in this paper the capillarity was absent, what makes the problem to be invariant to scale transformations.

4. Model validation

4.1. Validation against progressive waves

Progressive waves are solutions of the principal equations (16)–(18) (or, equivalently, (1)–(3)) with a constant external pressure p_e, and stationary in a moving coordinate system. The velocity of its motion is the progressive wave's phase speed. If such solutions are known *a priori* they can be used as an effective tool for validation of the model.

It is only for the case of pure capillary or Crapper's waves [15] that such solutions can be written analytically. Other stationary solutions, first of all Stokes waves (progressive pure gravity waves on deep water) have previously been obtained with various degrees of approximation. The most accurate algorithm was developed by Drennan et al. [24]. To obtain stationary solutions with computer accuracy (crucial for the purpose of model validation), we developed an iterative algorithm that is based on operators of integration and generalized Hilbert transformation in Fourier space. It employs the Fourier transform method to calculate nonlinearities. This algorithm is described in detail in ChSh (Section 3) and in [50], both of which present the results for deep-water gravity and gravity-capillary waves. In the latter, results for the case of finite depth also are obtained. These solutions as well as Crapper's waves may be considered exact – and were used for validation of the non-stationary model (system (32), (33)).

Employment of the periodicity condition (5) for the velocity potential (rather than the weaker condition of periodicity for the velocity components) assumes a zero mean velocity at the lower boundary. From this it follows that the mean over x velocity is zero at any level z that does not intersect the surface. Consequently, a progressive wave is not stationary in the model's coordinate system but propagates with a specific phase velocity. Such waves were simulated starting from initial conditions obtained as stationary solutions in a moving (bound to phase of the wave) coordinate system. If the resolution in the horizontal is high enough, and if the simulated wave is stable with respect to truncation errors, it should propagate indefinitely without changes of shape, and its phase velocity should be equal to its a priori known exact value. The model was validated against three types of waves: pure capillary deep-water (Crapper's) waves (which are analytical solutions); pure gravity and gravity-capillary waves derived numerically with the algorithm referred to above. Note that such validation is quite informative, since a non-stationary simulation "does not know" that the stationary solution obtained in a moving coordinate system with a different method must be a progressive wave in a resting coordinate system.

A detailed discussion of long-term validation runs can be found in ChSh. For all test cases, visual comparison of instantaneous wave profiles obtained during the simulations showed that the wave profiles moved with no spurious perturbations. To estimate "steadiness" of the numerical solution quantitatively, we calculated the phase velocities and amplitudes of the Fourier components for consecutive moments of time and obtained their temporal means and standard deviations over the period of integration. Results in ChSh (Table 4) show that even in the cases of steep waves, the calculated phase velocities were very close to their exact values (i.e. those obtained for the stationary solutions) for all three types of waves. Since conservation of the amplitudes was also very accurate (deviations of values during the simulations from their initial values retained less than 10^{-7} for the Stokes wave, and less than 10^{-11} for the capillary and gravity-capillary waves), the modes retained their initial energies and remained consistent in phase. Consequently, the simulated waves did not change their shapes during the integration. This result confirms that these waves are stable with respect to truncation errors, and that the numerical solutions yielded by the model approximate the solutions of the original differential equations with high accuracy.

It is known that for a precise description of steep Stokes waves a very large number of modes is needed [24]. An algorithm for precise calculation of Stokes waves based on conformal mapping was developed in ChSh. We used this algorithm for calculation of steep Stokes waves with an accuracy 10^{-11}. Here we present some new results on validation of our scheme by simulating very steep Stokes waves with amplitudes $a = 0.42$ and $a = 0.427$ (a is a half of the trough-to-crest height). $M = 1000$, $\Delta\tau = 0.001$ was used for numerical integration for the case $a_k = 0.42$, and $M = 4000$, $\Delta\tau = 0.0005$ for the case $a = 0.427$. The number of Fourier modes (constituents of Stokes wave), providing such accuracy, was about 100 and 150, correspondingly. Evolution of those Fourier amplitudes a_k of different constituents of Stokes wave which exceed 10^{-7} is shown in Fig. 1. In the first case, the Fourier amplitudes remain constant with very high accuracy. Slight oscillations of the Fourier amplitudes in the case of $a = 0.427$ reflect the approach to the critical value of $a = a_{cr} \approx 0.429$ corresponding to the Stokes wave with the maximum energy. For $a > a_{cr}$, Stokes waves exhibit unsteadiness, this is manifested in the finite-amplitude oscillations of the Fourier components (but not in breaking, as observed in the cases of $a = 0.43$ and $a = 0.44$, (not shown here) and is irrelevant for validation purposes). These integrations can be continued indefinitely without noticeable changes of the amplitudes or of the shape of the simulated Stokes wave for the case $a = 0.42$ and without changing the modulations for the case $a = 0.427$. Note that Dold's [19] simulation of the Stokes wave $a = 0.42$ collapse quickly.) Not unpredictably, for Stokes waves with amplitudes $a < 0.42$ the stability of solution is larger. For example, for $a = 0.35$ ($M = 1000$, $\Delta\tau = 0.001$), integration continued through several thousands periods of Stokes wave without noticeable fluctuations of amplitudes up to $k = 500$. Formally, stationary solution can be obtained also for $a = 0.44$. If such wave is used as a boundary condition in the non-stationary problem, the irregular oscillations arise in the vicinity of sharp crests. These oscillations finally disappear due to smoothing (48). After this moment, the wave remains virtually unchanged.

4.2. Convergence of the numerical solutions

If the proper stability requirements are met for a given initial condition, the numerical solutions obtained on a finite time interval should converge to the exact solution when the spatial resolution (truncation number M) goes to infinity. A model solution is trustworthy, if it does not differ markedly from solutions starting with the same initial condition obtained with higher resolutions. For all simulations described in the next section, we compared the results with those obtained with a doubled truncation number M. Except where we intentionally chose a too low resolution (see discussion of the special case in run 6, in the next section), the differences between the solutions presented and their versions obtained with M twice as large were negligible. This indicates that the corresponding wave profiles visually coincided for all moments of

Table 1
Characteristics of numerical experiments

Run no.	1	2	3	4	5	6
Initial conditions	$h = 0.5\cos x$	$h = 0.3\sin x$	$h = 0.28\cos x$	$h = 0.27\cos x$	$h = 0.01(\cos 10x + \cos 11x)$	$h = 0.04\cos(5x + \sin x)$
Resolution	$M = 3072$, $N = 13824$	$M = 6144$, $N = 27648$	$M = 3072$, $N = 13824$	$M = 1536$, $N = 6912$	$M = 12288$, $N = 55296$	$M = 3072$, $N = 13824$
Time step	$\Delta t = 5\times10^{-4}$	$\Delta t = 2.5\times10^{-4}$	$\Delta t = 5\times10^{-4}$	$\Delta t = 10^{-3}$	$\Delta t = 5\times10^{-4}$	$\Delta t = 10^{-3}$
Integration time	$T = 3.15$	$T = 5.58$	$T = 7.11$	$T = 500$	$T = 51.01$	$T = 37.44$
Comments	Breaking	Breaking	Breaking	No breaking	Breaking	Breaking

time shown in the figures – actually, during the *entire* integration periods excepting a very brief interval immediately preceding collapse of the solution, due to wave breaking.

Given a sufficiently high resolution, the numerical integrations presented here were capable of simulating individual wave breaking events. Such an event causes termination of the potential flow solution. The numerical dissipation (47) and (48) had negligible impact on energy; if not, differences from the higher resolution integrations would not have been insignificant. In contrast, model dissipation in the long-term simulations of multi-mode wave fields discussed in ChSh (Section 6) prevented some weak wave breaking events and, thus actually served as a parameterization of wave breaking. Still, if energy and steepness is large enough, the dissipation (46)–(48) is ineffective. It is why we made an attempt to introduce additional highly selective smoothing algorithm, which we briefly discuss in Section 6. The cases, which were terminated by instabilities exhibited the noticeable growth of high frequency part of spectrum, affected by dissipation (46)–(48). The waves approaching to breaking will imminently break, but precise moment of termination depends at some degree on resolution and time step of the scheme. For this reason, convergence in terms of instantaneous wave profiles could not take place for numerical solutions affected by dissipation, although the integral and spectral characteristics that were under investigation did conserve with a resolution increase.

5. Simulation of steep waves

The authors applied the method here described to simulate the nonlinear evolution of deep-water gravity waves (with the external pressure $p_e = 0$) and the initial stages of their breaking.[2] Two groups of model runs were carried out (Table 1): integrations starting from monochromatic waves of different amplitudes (runs 1–4), then with the initial wave profiles representing amplitude (run 5) and phase (run 6) modulation. For cases 1–6 the wave period was about 2π; for cases 5 and 6 linear estimations for group periods were 40.7 and 5.1, respectively.

Integration time T in the table may be compared with periods of the simulated waves. In linear approximation, these periods are: 2π for runs 1–4, $2\pi/\sqrt{10}$ for run 5, and $2\pi/\sqrt{5}$ for run 6. For all runs except run 4, T is the time for collapse of the numerical solution is closely identified with the time of existence of the potential flow solution (see discussion of convergence, previous section). For the solution in run 4, the time of existence is infinity.

For all cases, the initial surface velocity potential was constrained, so that, in linear approximation, the waves would propagate in the positive direction. According to linear theory for pure gravity waves ($\sigma = 0$)

[2] Obviously, a breaking wave, as a solution to the potential flow equations, a breaking wave only exists for a limited time interval. A potential flow model is thus unable to reproduce later stages of wave breaking that occur after the potential flow solution collapses and the actual flow becomes rotational and turbulent.

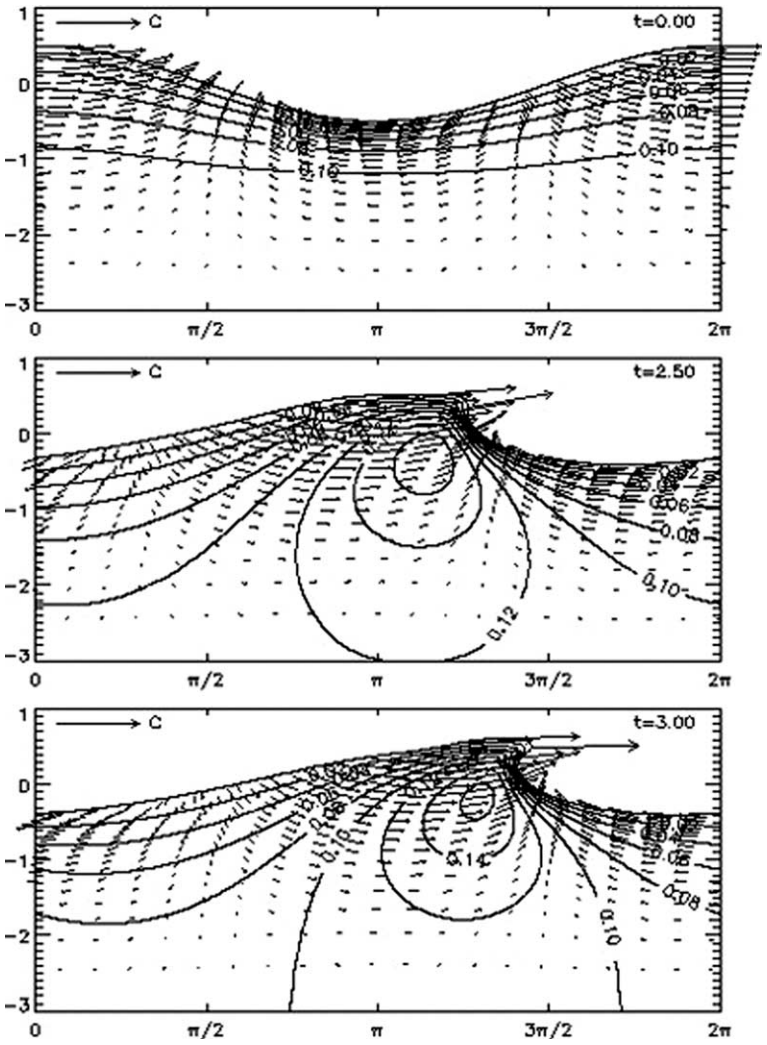

Fig. 2. Surface profiles, velocity vector fields (scaled by the linear phase velocity of the base wave shown at the left upper corner of each panel) and deviations of pressure from its generalized hydrostatic component (contour lines) for the initially monochromatic wave with maximum slope $a = 0.5$ (run 1). Times t indicated in right upper corners.

on deep water ($H = \infty$), this is ensured by the following relations for the Fourier coefficients of the initial data:[3]

$$\phi_k = \eta_{-k}\mathrm{sign}(k)/\sqrt{|k|}. \tag{50}$$

[3] See ChSh for the general case of finite-depth gravity-capillary waves. Here ϕ_k and η_k are the Fourier coefficients of the surface velocity potential and surface height, respectively. The Fourier expansion is that over the Cartesian coordinate x, rather than the new horizontal coordinate ξ (cf. (11) and (21)). However, there is no difference between the two types of expansion from the point of view of linear theory.

As a test of the model's ability to simulate the evolution of very large waves, we first chose initial data chose was somewhat unrealistic, namely a monochromatic wave with the maximum slope (non-dimensional amplitude) $a = \max(h_x) = 0.5$. The results are shown in Fig. 2, where the instantaneous surface height profiles, velocity fields, and deviations of pressure from its generalized hydrostatic component (i.e. $p + \zeta$, according to Section 2) are depicted for different moments of time. Initial conditions are shown in the upper panel; the middle panel corresponds to the moment when the maximum slope $\max|h_x|$ becomes infinite (the overturning begins). The lower panel represents a condition approaching collapse, with overturning already in an advanced stage. Note the pressure "bubble" in the middle panel, which becomes somewhat less pronounced later, when the "excessive mass" of the overturning crest is on the merge of release. As well, results also illustrate a further advantage of the conformal mapping method: ability to reproduce surface height profiles that are multi-valued functions of the horizontal coordinate x. This becomes possible because, with $\zeta = 0$, formulae (9) and (10) serve as a parametric representation of the surface.

In Fig. 3, the same instantaneous fields are presented for the case of the initially monochromatic wave, with $a = 0.3$ (run 2). This wave, too, eventually breaks but only a relatively small portion of mass near the peak that overturns. Unlike the previous case, when the overturning begins ($t = 5.45$) the crest sharpens dramatically, rendering the overturning stage short-lived; simulation of this effect required a higher resolution than in run 1. The middle panel of Fig. 3 depicts the wave well before its overturning but with a high-pressure area beneath the crest well developed along with other features of nonlinear behavior – such as sharpening of the crest, increasing height (more than 1.6 times initial value), and large velocities at the crest. The lower panel represents a short period between the beginning of overturning and collapse of the solution. At this stage, as well as during the breaking stage in run 1, the velocities at the crest exceed the (linear) phase velocity by 1.1–1.3 times.

Time evolution of the maximum slope $\max|h_x|$, maximum velocity $\max|\vec{V}| = \max\left(\sqrt{\Phi_x^2 + \Phi_z^2}\right)$, maximum surface height $\max(h)$, and the wave height $\Delta h = \max(h) - \min(h)$ is shown in Figs. 4 and 5 for the cases of initially monochromatic waves with $a = 0.28$ (run 3) and $a = 0.27$ (run 4). Again, both waves' behavior is highly nonlinear, and, during an initial stage of about one wave period, each exhibits quantitatively similar growth, a steepening, and acceleration at the crest. However, whereas this initial evolution results in breaking for the former similar to run 2, the latter wave survives its climax. Its characteristics reverse their tendencies to reach a low close to initial values and, then, continue to oscillate in a quasi-periodic manner. This suggests that for initially monochromatic waves, the critical value a^* of the initial amplitude (such that waves with $a > a^*$ eventually break whereas those with $a < a^*$ do not) lies between 0.27 and 0.28.[4] Note that these conclusions were obtained with a high resolution scheme, and influence of dissipation shifted to very high frequencies was negligible.

The wave in run 4 is thus close to the highest non-breaking initially monochromatic wave. It is worth mentioning that the maxima of height Δh (about 0.62, see the lowest panel, Fig. 4), let alone its initial height $2a = 0.54$, are considerably less than the height of the steepest Stokes wave (0.886) or the Stokes wave of maximal energy (0.858). Likewise, the total energy of the wave in run 4 is only about 0.50 the maximum energy of Stokes waves. So the latter's characteristics cannot serve as breaking criteria.

It is noteworthy that for all simulations with initially monochromatic waves, growth of the maximum surface height (crest height) $\max(h)$ significantly exceeded growth of the wave height Δh (see Figs. 2 and 3; cf. 3rd and 4th panels, Figs. 4 and 5) Sharpening of the crest was accompanied by a flattening of the trough. The wave was thus increasing its skewness. For non-breaking waves, these processes turn out to be fully reversible (run 4, Fig. 5). It is interesting that values of Jacobian less than $J = 0.2$ were never observed. Hence, a division to J in Eqs. (33) and (34) did not play significant role in instability. On the con-

[4] This estimate may be different if the initial velocity potential is not prescribed according to Eq. (50).

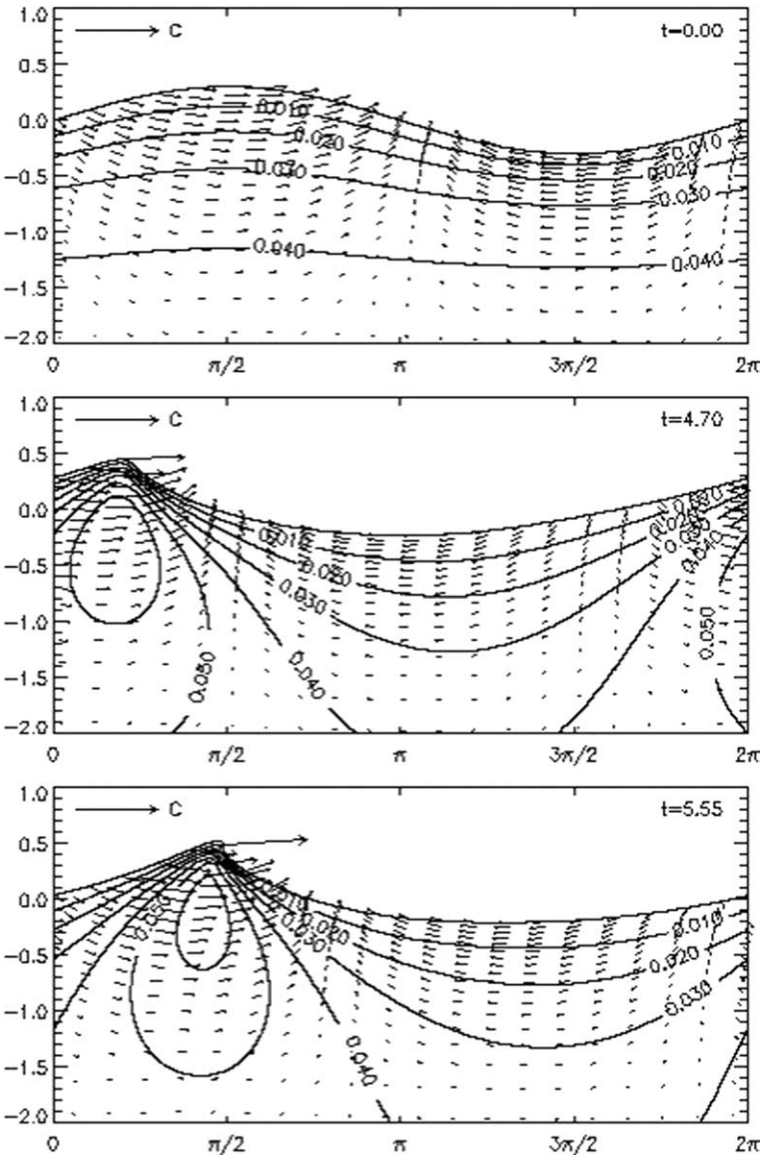

Fig. 3. Same as in Fig. 1 but with $a = 0.3$ (run 2).

trary, very large values of J in vicinity of sharp crests (up to $J = 100$) were typical. It did not influence directly the stability, but imposed the additional restrictions to time step $\Delta\tau$.

Runs 5 and 6 simulate nonlinear evolution of wave fields that have a relatively low initial maximum slope $\max|h_x|$ (0.209 and 0.239, respectively) and yet result in emergence of steep breaking waves. In run 5, the initial condition is a superposition of two monochromatic waves with the same amplitude and close wave numbers; it may be rewritten as $h = 0.02\cos 0.5x\cos 10.5x$ and so represents a "single" wave with slowly changing amplitude. The results are presented in Fig. 6 (instantaneous fields) and Fig. 7 (time evolution of geometric characteristics). Note that whereas a monochromatic wave overturns in about one wave

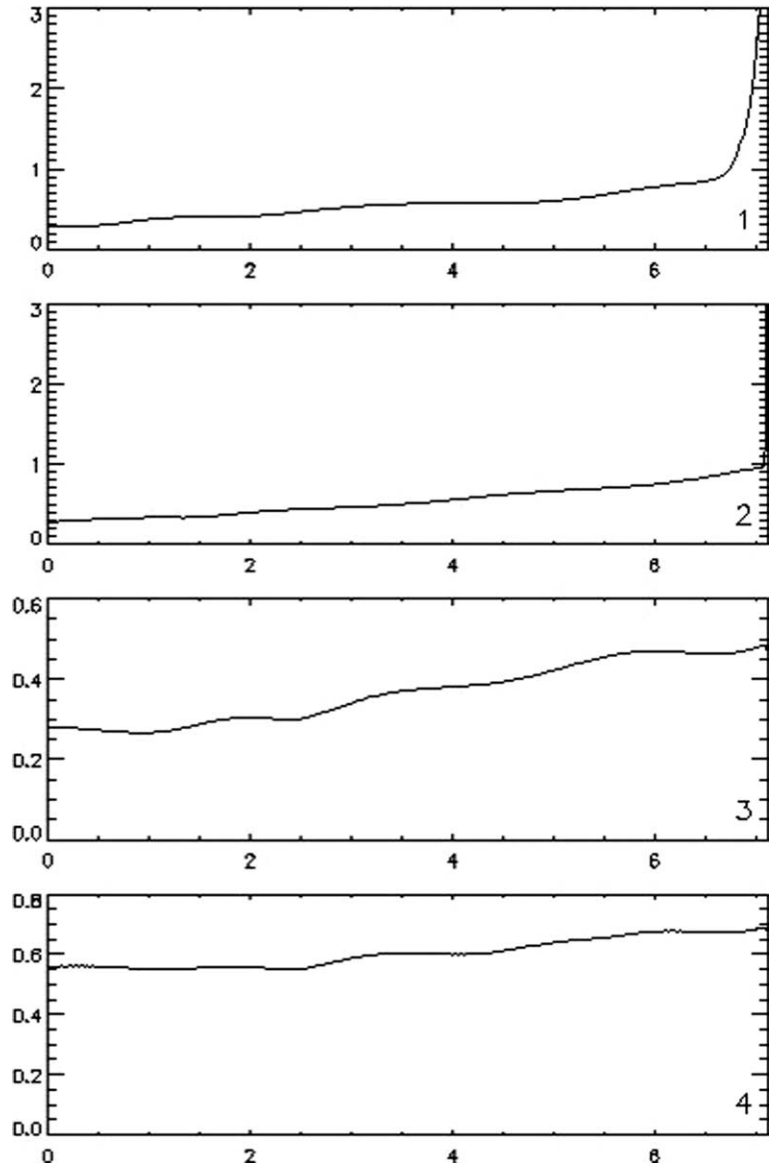

Fig. 4. Temporal evolution of geometric characteristics of the initially monochromatic wave with $a = 0.28$ (run 3): 1 – maximum slope $\max|h_x|$; 2 – maximum velocity $\max|\vec{V}|$; 3 – maximum surface elevation $\max(h)$; 4 – wave height $\Delta h = \max(h) - \min(h)$.

period or less (if ever), it takes some 26 wave periods for the modulated wave in run 5 to reach the breaking. For the former case, an individual wave has enough initial energy to grow nonlinearly to break point. In the latter, an individual wave that eventually breaks does not have a "critical" initial energy but, instead, grows as a result of relatively slow energy redistribution along the wave train.

For run 6, the initial condition represents a phase (or frequency) modulation of the base wave with wave number $k = 5$. The results (Figs. 8 and 9) are similar to those for amplitude modulation (run 5): redistribution of energy along the wave train which continues for many periods of the base wave (13 periods, run 6).

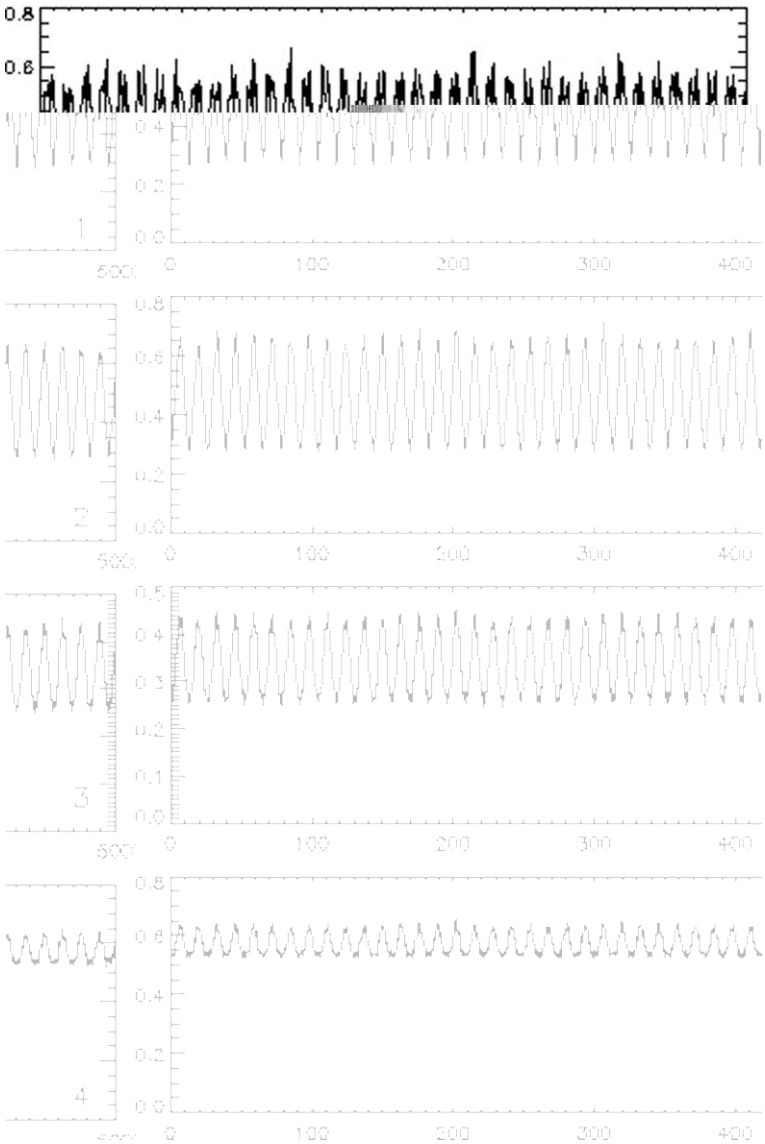

Fig. 5. Same as in Fig. 4 but with $a = 0.27$ (run 4).

This effect is clearly seen in Figs. 6 and 8; eventually it brings about formation of a very high breaking wave having a sharp crest where velocity exceeds the phase velocity. A deep trough follows, a high pressure area is formed under the crest, and the maximum surface elevation becomes about twice as large as its initial value (Figs. 6 and 8, lower panel).

A special feature of run 6 is that numerical simulation survives the first wave breaking event (Fig. 8, 2nd panel; note the corresponding maxima of geometric characteristics in Fig. 9). The critical stage begins at $t \approx 32.5$; the exact solution, for which the numerical solution with $M = 12288$ proves a close approximation, collapses at $t = 33.16$. However, this turns out to be a "mini-breaking" that affects only a tiny portion of the top of a sharp crest. A coarser resolution $M = 3072$, used in run 6, engenders

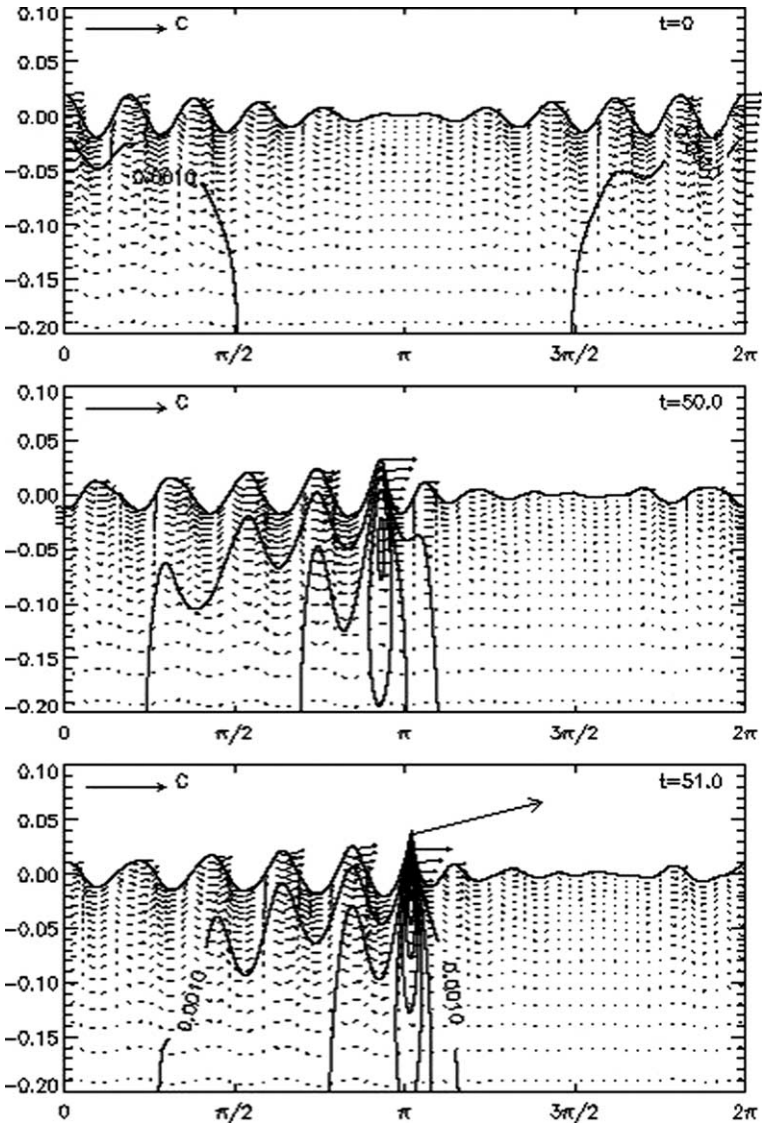

Fig. 6. Same as in Fig. 1 but a simulation starting from a base wave with an amplitude modulation (run 5).

greater numerical dissipation and allows the wave to absorb this event with a release of energy as small as 4×10^{-4} of its total value. Before the critical stage is reached, the solution practically coincides with that obtained with higher resolution. The artificially lowered resolution allows authors to follow wave train evolution beyond the first breaking, though with a lower accuracy. In Fig. 8 (3rd panel), the wave that formerly underwent breaking has somewhat subsided, whereas the following wave has become both sharper and higher. In the lowest panel, this wave exhibits a surface height maximum that is distinctly greater than that reached during the first breaking (Fig. 9, lower panel), as the crest sharpens and accelerates dramatically. At this point ($t = 37.40$), the wave is already in breaking stage; the numerical solution finally collapses at $t = 37.44$.

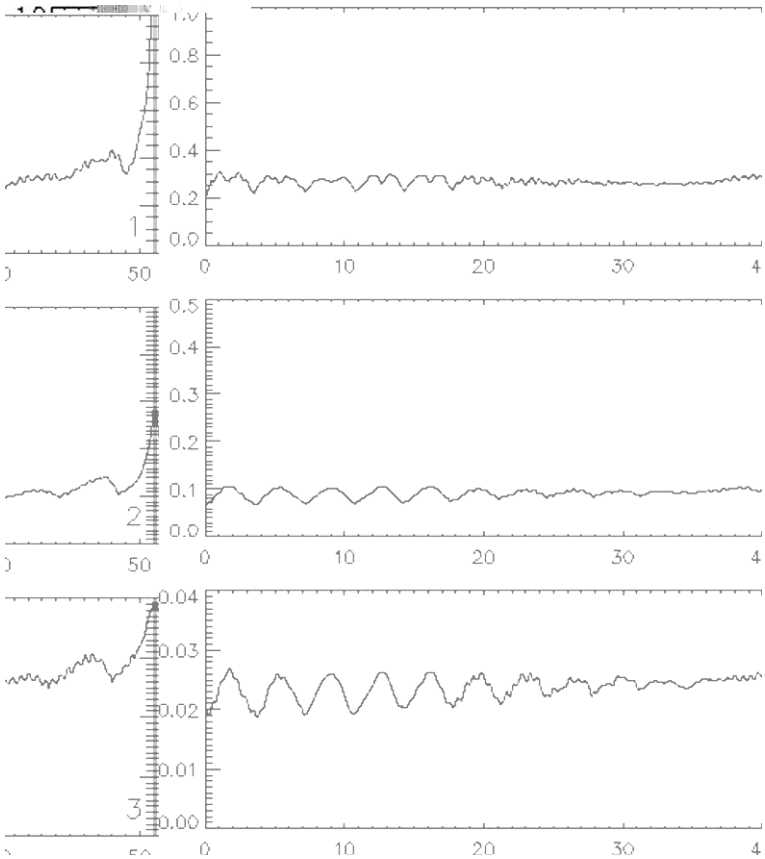

Fig. 7. Temporal evolution of geometric characteristics for the simulation starting from a base wave with an amplitude modulation (run 5): 1 – maximum slope max$|h_x|$; 2 – maximum velocity max $|\vec{V}|$; 3 – maximum surface elevation max(h).

6. Wave breaking

In recent years, great attention has been paid to effects of wave breaking. Our particular way of modeling based on conformal mapping, allows us to approach very closely the breaking point where the potential solution ceases to exist. In such cases, integration is always terminated. However, in this instance given its high accuracy, the scheme is capable of following the developing physical instabilities very closely during the *entire period of existence of the potential solution*. When overturning and breaking are investigated per se, the phenomena is simulated explicitly up to collapse. Beyond this point, breaking evidently is non-potential. And so the direct method is inapplicable to long-term simulations of wave fields with multiple breaking events, in particular to coupled modeling of WBL and simulations of wave drag and energy exchange between wind and waves.

To make such simulations possible, we developed a method of parameterization of breaking effects based on smoothing. Smoothing should be made locally in physical space. We explored many ways to parameterize this effect. The best scheme is based on a simple diffusion-type algorithm with the coefficient of diffusion depending on the second horizontal derivative of the surface height:

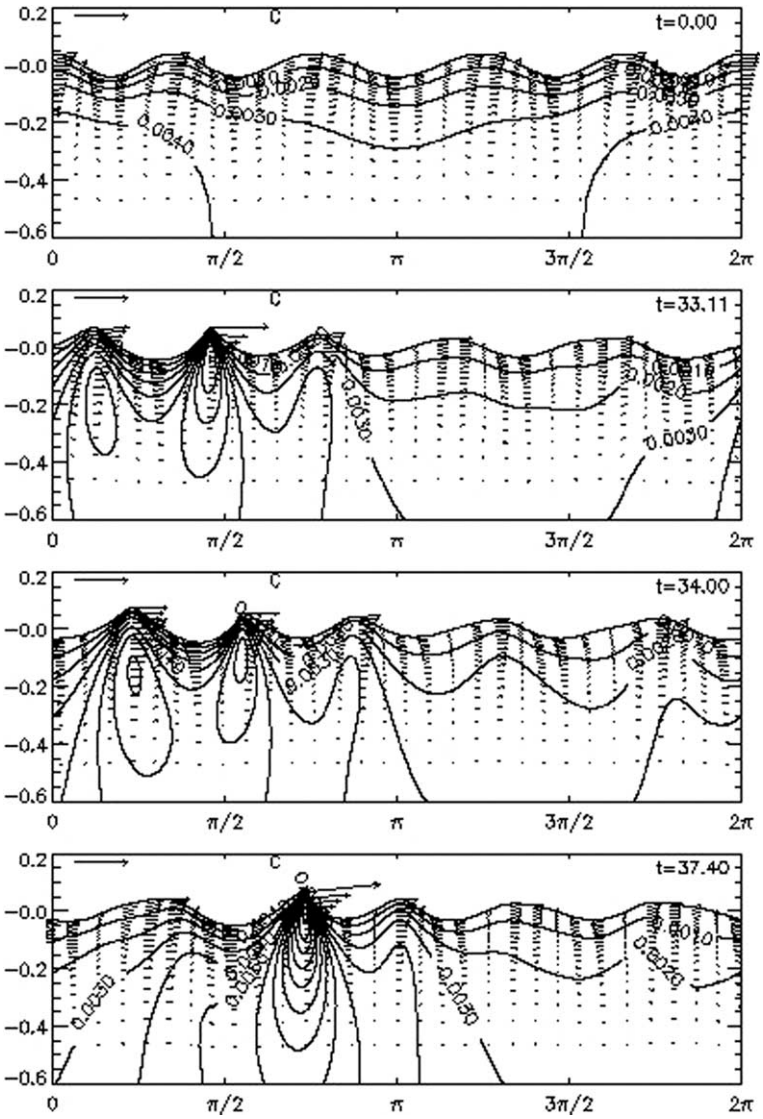

Fig. 8. Same as in Fig. 1 but for the simulation starting from a base wave with a phase modulation (run 6).

$$z_\tau = F_z + J^{-1}\frac{\partial}{\partial\xi}B\frac{\partial z}{\partial\xi}, \tag{51}$$

$$\Phi_\tau = F_\Phi + J^{-1}\frac{\partial}{\partial\xi}B\frac{\partial \Phi}{\partial\xi}, \tag{52}$$

where F_z and F_Φ are the right-hand sides in Eqs. (32) and (33), and

$$B = \begin{cases} C_b\left(\frac{2\pi}{N}\frac{\partial^2 z}{\partial\xi^2}\right)^2, & \frac{\partial^2 z}{\partial\xi^2} > s, \\ 0, & \frac{\partial^2 z}{\partial\xi^2} \leqslant s, \end{cases} \tag{53}$$

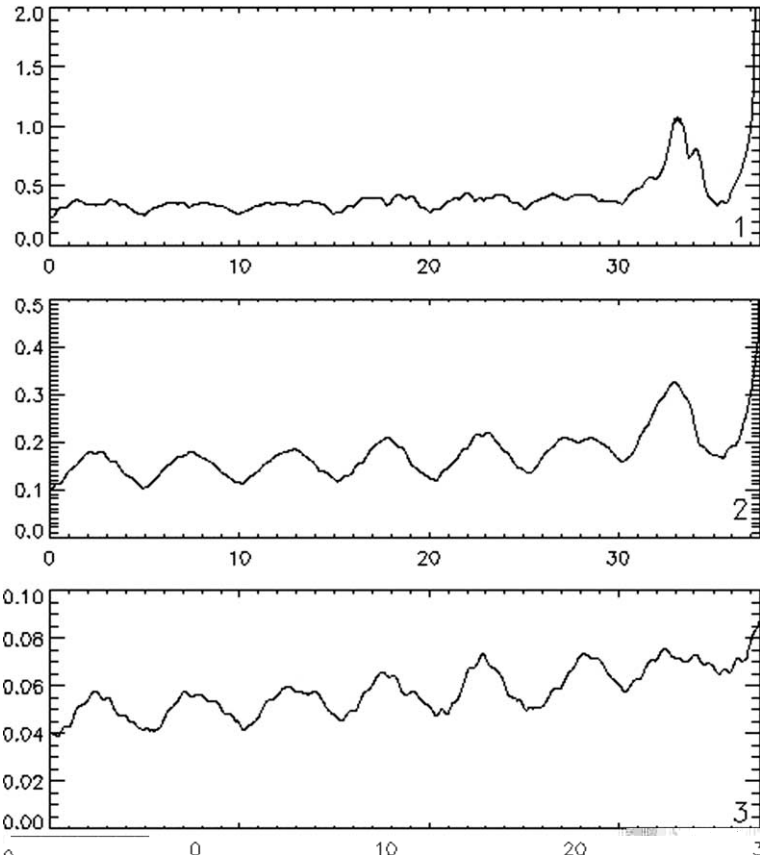

Fig. 9. The same as in Fig. 6 but for the simulation starting from a base wave with a phase modulation (run 6).

where coefficient C_b is of the order of 10^{-2}, and the critical value of the second derivative s is of the order of 100. The empirical condition (53) is introduced to leave non-breaking waves unaffected. The algorithm (51)–(53) does not change the volume but does decreases the energy and momentum (Figs. 10 and 11). It is implicitly assumed that both the lost energy and momentum are transferred partly to the flow and partly to turbulence (these transitions may be separated, as in [11]).

This parameterization of the impact of rotational breaking effects on the potential component of flow allows us to prevent development of breaking. Further, this approach does not noticeably influence the solution when breaking does not develop. We do not consider this algorithm as a final solution to the problem; however, as it cannot prevent the numerical solution from collapsing when initial steepness or energy is very large. But for typical steepness of sea waves and in cases when growth of energy occurs relatively slowly, the scheme works satisfactorily.

On average, 1-D wave spectrum S at high wave numbers in quasi-stationary regime decays as k^{-6}–k^{-5} – much faster than it was obtained for 2-D case. Numerical experiments performed by Onorato et al. [45]) based on a Dommermuth and Yue [22] scheme obtained that S decaying as $k^{-2.5}$ for 2-D waves. Differences such as these arise because the nonlinearity in 1-D waves is much weaker that for 2-D waves. Fast decaying of the spectrum for 1-D waves is a primary disadvantage of 1-D approach.

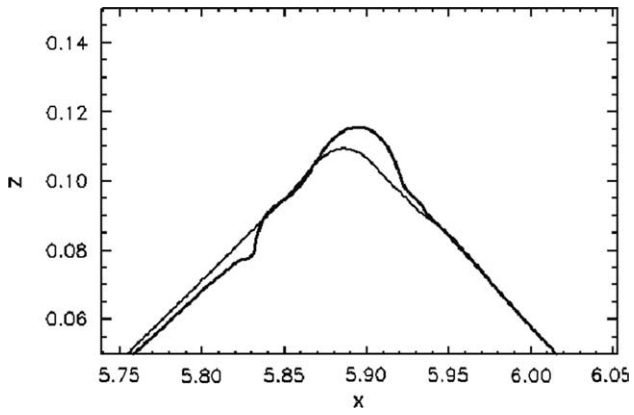

Fig. 10. Fragment of a wave surface affected by breaking adjustment algorithm: thick line is surface at $t = 2.16$ with no breaking adjustment; thin line is surface at the same moment but simulated with breaking adjustment.

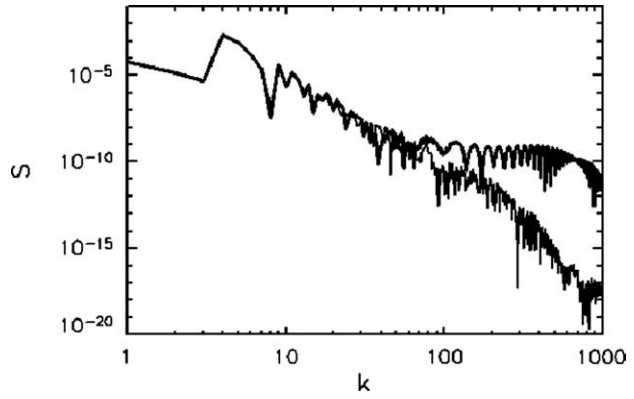

Fig. 11. Spectrum of waves at $t = 2.16$: thick line – no breaking adjustment; thin line – with included breaking adjustment.

7. Discussion and conclusions

In this study, we applied the method for numerical simulation of surface waves developed in ChSh to modeling of steep gravity waves in deep water. The principal equations are the standard equations of hydrodynamics for potential flow with a free surface. The method is based on a non-stationary conformal transformation that maps the original domain (which may be of finite or infinite depth) onto a domain with a fixed rectilinear upper boundary; for the stationary problem, the method is identical with the classic complex variable method. In the transformed coordinates, the solution to the Laplace equation for the velocity potential is written out as a Fourier series, which eliminates the need for a finite-difference approximation of spatial derivatives, thus reducing the problem to 1-D. Numerical solution of the initial value problem for the transformed system thus proves straightforward, reduced to time integration of two simple evolutionary equations for the surface velocity potential and surface height. These variables are represented by their Fourier expansions with time-dependent coefficients. The Fourier transform method used for calculation of the nonlinear terms provides high computational efficiency; the number of arithmetic operations per time step is of the order $M \ln M$, where M is the truncation number. Rigorous validation of this method included tests on convergence of the numerical solutions with $M \to \infty$ as well as long-term runs with initial condi-

tions taken from a priori known progressive wave solutions. The results of these tests allow us, for any practical purpose, to identify the numerical solutions considered in this paper with exact solutions – almost up to the moment when the (exact) solution collapses because due to wave breaking. The method is applicable to simulation of the initial stage of wave overturning, when the surface becomes a multi-valued function of the (Cartesian) horizontal coordinate.

Evolution of an initially monochromatic wave is one of the simplest examples of nonlinear interaction. Our simulations show that such waves exhibit growth in height, still greater growth of crest height, a sharpening and acceleration of the crest, and a flattening of the trough. With the initial maximum slope $a \leqslant 0.27$, such waves do not break; further, the behavior of their geometric characteristics is quasi-periodic in time. Accordingly, these tendencies are fully reversible. If $a \geqslant 0.28$, the process results in wave breaking, which occurs within about one wave period or less. The overturning is well reproduced in the simulations and is especially impressive for larger waves - reminiscent a ''wall of water'', reported by sailors. The quantitative estimate of the critical a may depend on exactly how we define the velocity potential of the initial monochromatic wave; in this case, the potential was represented by one Fourier component (as was the surface height) whose phase was determined so that the wave propagated in one direction.

Also considered were two cases of wave fields with more complex initial conditions. One was two Fourier components with close wave numbers, that is a base wave with an *amplitude* modulation. The other initial condition was a base wave with a *phase* modulation. Both simulations were characterized by a redistribution of energy along the wave train, a process which persisted for many periods and resulted in formation of large steep breaking waves having sharp crests. Qualitatively, the outputs described are close to observed extreme waves [40].

The model herein developed may be applied to a broad range of situations where the 1-D approximation is acceptable. Unless proper parameterizations are used, it cannot be used to simulate processes in which *weak* (irreversible) 2-D nonlinear interactions are of essence. However, many wave phenomena are controlled largely by strong nonlinear interactions which are relatively fast and for which the 1-D approximation is often adequate. Formation of extreme waves is one such phenomena. We emphasize that model simulations of these waves exceeds far academic interest only. It has long been known that nonlinear redistribution of energy is characteristic for wave trains and may, on occasion, result in sudden emergence of very large, steep waves known as freak or rogue waves. Amplitude and phase modulations create especially favorable conditions for the formation of such waves. The case studies carried out in this paper illustrate the model's ability to simulate these phenomena.

Other applications of the scheme developed here include simulations of multi-wave fields, including coupled modeling of waves and a wave boundary layer [6], and studies of shallow water waves [50].

Acknowledgment

The authors wish to thank William F. Althoff, Research Associate, Smithsonian Institution, who edited the paper and made a number of improvements as well as unknown reviewers for their valuable comments and suggestions.

References

[1] G.R. Baker, D.I. Meiron, S.A. Orszag, Generalized vortex methods for free-surface flow problems, J. Fluid Mech. 123 (1982) 477–501.

[2] M.L. Banner, X. Tian, On the determination of the onset of breaking for modulating surface gravity waves, J. Fluid Mech. 367 (1998) 107–137.

[3] W.J.D. Bateman, C. Swan, P.H. Taylor, On the efficient numerical simulation of directionally spread surface water waves, J. Comput. Phys. 174 (2001) 277–305.
[4] S.E. Belcher, J.C.R. Hunt, Turbulent flow over hills and waves, Ann. Rev. Fluid Mech. 30 (1998) 507–538.
[5] H. Bredmose, M. Brocchini, D.H. Peregine, L. Tsais, Experimental investigation and numerical modeling of steep forced water waves, J. Fluid Mech. 490 (2003) 217–249.
[6] D. Chalikov, Interactive modeling of surface waves and boundary layer, Ocean Wave Measurements and Analysis, ASCE, in: Proceeding of the third International Symposium on WAVES 97, 1998, pp. 1525–1540.
[7] D. Chalikov, The numerical simulation of wind–wave interaction, J. Fluid Mech. 87 (1978) 551–582.
[8] D.V. Chalikov, Yu.M. Liberman, Integration of primitive equations for potential waves, Izv. Sov. Atmos. Ocean Phys. 27 (1991) 42–47.
[9] D. Chalikov, D. Sheinin, The numerical investigation of wavenumber-frequency spectrum for 1-D nonlinear waves, in: WMO/ISCU, 1994, CAS/JSC Working Group on Numerical Experimentation, vol. 19, WMO/TD, 1994, p. 592.
[10] D. Chalikov, D. Sheinin, Numerical investigation of wavenumber-frequency spectrum for 1-D nonlinear waves, in: 1994 Ocean Sciences Meeting, San-Diego, CA, February 21–25, Abstract in: EOS, transactions (supplement), AGU, vol. 75, 1994, p. 100.
[11] D. Chalikov, M. Belevich, One-dimensional theory of the wave boundary layer, Bound. Layer Met. 63 (1992) 65–96.
[12] D. Chalikov, D. Sheinin, Numerical modeling of surface waves based on principal equations of potential wave dynamics, Technical Note NOAA/NCEP/OMB, 1996, 54 pp.
[13] D. Chalikov, D. Sheinin, Direct modeling of one-dimensional nonlinear potential waves, in: W. Perrie (Ed.), Nonlinear Ocean Waves, Advances in Fluid Mechanics, vol. 17, 1998, pp. 207–258.
[14] W. Craig, C. Sulem, Numerical simulation of gravity waves, J. Comput. Phys. 108 (1993) 73–83.
[15] G.D. Crapper, An exact solution for progressive capillary waves of arbitrary amplitude, J. Fluid Mech. 96 (1957) 417–445.
[16] G.D. Crapper, Introduction to Water Waves, John Wiley, Chichester, 1984, 224 pp.
[17] A.A. Dimas, G.S. Triantafyllou, Nonlinear interaction of shear flow with a free surface, J. Fluid Mech. 260 (1994) 211–246.
[18] J.W. Dold, D.H. Peregrine, A efficient boundary-integral method for steep unsteady water waves, in: K.W. Morton, M.J. Baines (Eds.), Numerical Methods for Fluid Dynamics, Oxford University Press, Oxford, 1986.
[19] J.W. Dold, An efficient surface-integral algorithm applied to unsteady gravity waves, J. Comput. Phys. 103 (1992) 90–115.
[20] D.G. Dommermuth, D.K.P. Yue, R.J. Rapp, F.S. Chan, W.K. Melville, Deep waterbreaking waves; a comparison between potential theory and experiments, J. Fluid Mech. 89 (1988) 432–442.
[21] D.G. Dommermuth, The laminar interactions of a pair of vortex tubes with a free surface, J. Fluid Mech. 246 (1993) 91–115.
[22] D.G. Dommermuth, D.K.P. Yue, A high-order spectral method for the study of nonlinear gravity waves, J. Fluid Mech. 184 (1987) 267–288.
[23] M.A. Donelan, Air–sea interaction, in: B. LeMehaute, D.M. Hanes (Eds.), The Sea, 9, Ocean Engineering Science, Wiley–Interscience, 1990, pp. 239–292.
[24] W.M. Drennan, W.H. Hui, G. Tenti, Accurate calculation of Stokes wave near breaking, in: C. Graham, S.K. Malik (Eds.), Continuum Mechanics and its Applications, Hemisphere Publishing, Washington, DC, 1988.
[25] A.I. Dyachenko, E.A. Kuznetsov, M.D. Spector, V.E. Zakharov, Analytical description of the free surface dynamics of an ideal fluid (canonical formalism and conformal mapping), Phys. Lett. A 221 (1–2) (1996) 73–79.
[26] E.B. Eliassen, B. Machenhauer, E. Rasmussen, On a numerical method for integration of the hydro-dynamical equations with a spectral representation of the horizontal fields, Report 2, Institute for Teoretisk, Meteorologi, Kobenhavens Universitet, Copenhagen, 1970.
[27] J. Farmer, L. Martinelli, A. Jameson, A Fourier method for solving nonlinear water-wave problems: application to solitary–wave interactions, J. Fluid Mech. 118 (1993) 411–443.
[28] J.D. Fenton, M.M. Rienecker, A Fourier method for solving nonlinear water-wave problems: application to solitary–wave interactions, J. Fluid Mech. 118 (1982) 411–443.
[29] B. Fornberg, A numerical method for conformal mapping, SIAM, J. Sci. Comput. 1 (1980) 386–400.
[30] M.J. Fritts, M.J. Meinhold, C.H. von Kerczek, The calculation of nonlinear bow waves, in: Proceedings of the 17th Symposium on Naval Hydrodynamics, The Hague, Netherlands, 1988, pp. 485–497.
[31] P.R. Gent, P.A. Taylor, A numerical model of the air flow above water waves, J. Fluid Mech. 77 (1976) 105–128.
[32] F.H. Harlow, E. Welch, Numerical calculation of time-dependent viscous incompressible flow of fluid with free surface, Phys. Fluids 8 (1965) 2182–2189.
[33] K.L. Henderson, D.H. Peregrine, J.W. Dold, Unsteady water waves modulations: fully nonlinear solutions and comparison with the nonlinear Shroedinger equation, Wave Motion 29 (1999) 341–361.
[34] J.M. Hyman, Numerical methods for tracking interfaces, Physica D 12 (1984) 396–407.
[35] J.M. Floryan, H. Rasmussen, Numerical methods for viscous flows with moving boundaries, Appl. Mech. Rev. 42 (1989) 32341.
[36] C.W. Hirt, B.D. Nichols, Volume of fluid method for the dynamics of free surface, J. Comput. Phys. 39 (1981) 201–225.
[37] T. Kano, T. Nishida, Sur le ondes de surface de l'eau avec une justification mathematique des equations des ondes en eau peu profonde, J. Math., Kyoto Univ. (JMKYAZ) 19-2 (1979) 335–370.

[38] M.S. Longuet-Higgins, E.D. Cokelet, The deformation of steep surface waves on water. I. A numerical method of computation, Proc. R. Soc. London 350 (1976) 1–26.
[39] M.S. Longuet-Higgins, D.G. Dommermuth, Crest instabilities of gravity waves. III. Nonlinear development and breaking, J. Fluid Mech. 336 (1997) 33–50.
[40] A.K. Magnusson, M.A. Donelan, W.M. Drennan, On estimating extremes in an Evolving Wave Field, Coastal Eng. 36 (1999) 147–163.
[41] C.C. Mei, Numerical methods in water-wave diffraction and radiation, Annu. Rev. Fluid Mech. 10 (1978) 393–416.
[42] D.I. Meiron, S.A. Orszag, M. Israeli, Applications of numerical conformal mapping, J. Comput. Phys. 40 (2) (1981) 345–360.
[43] H. Miyata, Finite-difference simulation of breaking waves, J. Comput. Phys. 5 (1986) 179–214.
[44] W.F. Noh, P. Woodward, SLIC (simple line interface calculation), in: Lecture Notes in Physics 59 (1976) 330–340, Springer-Verlag, New York.
[45] M. Onorato, A.R. Osborn, M. Serio, D. Resio, A. Pushkarev, V.E. Zakharov, C. Brandini, Freely decaying weak turbulence for sea-surface gravity waves, Phys. Rev. Lett. 89 (2002) 144501-1–144501-4.
[46] S.A. Orszag, Transform method for calculation of vector coupled sums. Application to the spectral form of vorticity equation, J. Atmos. Sci. 27 (1970) 890–895.
[47] A. Prosperetti, J.W. Jacobs, A numerical method for potential flow with a free surface, J. Comput. Phys. 51 (1983) 365–386.
[48] A.J. Roberts, A stable and accurate numerical method to calculate the motion of a sharp interface between fluids, IMA J. Appl. Math. 1 (1983) 293–316.
[49] D. Sheinin, D. Chalikov, Numerical investigation of wavenumber-frequency spectrum for 1-D nonlinear waves, in: Office of Naval, Research (ONR) Ocean Waves Workshop, University of Arizona, Tucson, AZ, March 16–18, 1994. Extended abstract, 1994.
[50] D. Sheinin, D. Chalikov, Hydrodynamical modeling of potential surface waves – In: Problems of hydrometeorology and environment on the eve of XXI century, in: Proceedings of International Theoretical Conference, St. Petersburg, June 24–25, 1999, Hydrometeoizdat 2000 (2000) 305–337.
[51] J.-B. Song, M. Banner, On determining the onset and strength of breaking for deep water waves. Part 1: Unforced irrotational wave groups, J. Phys. Oceanogr. 32 (9) (2002) 2541–2558.
[52] G.G. Stokes, On the theory of oscillatory waves, Trans. Cambridge Philos. Soc. 8 (1847) 441–445; Math. Phys. Pap. 2 (1) (1847) 197–229.
[53] M. Tanaka, J.W. Dold, M. Lewy, D.H. Peregrine, Instability and breaking of a solitary wave, J. Fluid Mech. 187 (1987) 235–248.
[54] S. Tanveer, Singularities in water waves and Rayleigh-Taylor instability, Proc. R. Soc. Lond. A 435 (1991) 137–158.
[55] S. Tanveer, Singularities in the classical Rayleigh-Taylor flow: formation and subsequent motion, Proc. R. Soc. Lond. A 441 (1993) 501–525.
[56] J.F. Thompson, Z.U.A. Warsi, C.W. Mastin, Boundary-fitted coordinate systems for numerical solution of partial differential equations – a review, J. Comput. Phys. 47 (1982) 1–108.
[57] W.T. Tsai, D.K.P. Yue, Computation of nonlinear free-surface flows, Annu. Rev. Fluid Mech. 28 (1996) 249–278.
[58] T. Vinje, P. Brevig, Numerical simulation of breaking waves, Adv. Water Resour. 4 (1981) 77–82.
[59] K.M. Watson, B.J. West, A transport-equation description of nonlinear ocean surface wave interactions, J. Fluid Mech. 70 (1975) 815–826.
[60] B.J. West, K.A. Brueckner, R.S. Janda, A new numerical method for surface hydrodynamics, J. Geophys. Res. 92 (1987) 11803–11824.
[61] J.C. Whitney, The numerical solution of unsteady free-surface flows by conformal mapping, in: M. Holt (Ed.), Proceedings of the Second International Conference on Numer. Fluid Dynamics, Springer-Verlag, Berlin, 1971, pp. 458–462.
[62] V.E. Zakharov, A.I. Dyachenko, O.A. Vasilyev, New method for numerical simulation of a nonstationary potential flow of incompressible fluid with a free surface, Eur. J. Mech. B: Fluids 21 (2002) 283–291.
[63] M.A. Yeung, Numerical methods in free-surface flows, Annu. Rev. Fluid Mech. 14 (1982) 395–442.
[64] J. Zhang, K. Hong, D.K.P. Yue, Effects of wavelength ratio on wave modeling, J. Fluid Mech. 248 (1993) 107–127.